

University of Texas Rio Grande Valley

ScholarWorks @ UTRGV

Manufacturing & Industrial Engineering Faculty
Publications and Presentations

College of Engineering and Computer Science

5-24-2023

Experimental investigation of various energy-absorbing layer materials and sodium alginate viscosities on the jet formation in laser-induced-forward-transfer (LIFT) bioprinting

Shuqi Zhou

Chaoran Dou

Jianzhi Li

The University of Texas Rio Grande Valley

Qiqi Zhang

Qilin Dai

See next page for additional authors

Follow this and additional works at: https://scholarworks.utrgv.edu/mie_fac



Part of the [Industrial Engineering Commons](#), and the [Manufacturing Commons](#)

Recommended Citation

Shuqi Zhou, Chaoran Dou, Jianzhi Li, Qiqi Zhang, Qilin Dai, Ben Xu; Experimental investigation of various energy-absorbing layer materials and sodium alginate viscosities on the jet formation in laser-induced-forward-transfer (LIFT) bioprinting. *Journal of Applied Physics* 28 May 2023; 133 (20): 204701.
<https://doi.org/10.1063/5.0145737>

This Article is brought to you for free and open access by the College of Engineering and Computer Science at ScholarWorks @ UTRGV. It has been accepted for inclusion in Manufacturing & Industrial Engineering Faculty Publications and Presentations by an authorized administrator of ScholarWorks @ UTRGV. For more information, please contact justin.white@utrgv.edu, william.flores01@utrgv.edu.

Authors

Shuqi Zhou, Chaoran Dou, Jianzhi Li, Qiqi Zhang, Qilin Dai, and Ben Xu

RESEARCH ARTICLE | MAY 24 2023

Experimental investigation of various energy-absorbing layer materials and sodium alginate viscosities on the jet formation in laser-induced-forward-transfer (LIFT) bioprinting

Zhou Shuqi (周澍祺); Dou Chaoran (窦超然); Li Jianzhi (李建志); ... et. al



Journal of Applied Physics 133, 204701 (2023)

<https://doi.org/10.1063/5.0145737>



View
Online



Export
Citation

CrossMark



Time to get excited.

Lock-in Amplifiers – from DC to 8.5 GHz



Find out more

 Zurich Instruments

Experimental investigation of various energy-absorbing layer materials and sodium alginate viscosities on the jet formation in laser-induced-forward-transfer (LIFT) bioprinting

Cite as: J. Appl. Phys. **133**, 204701 (2023); doi: [10.1063/5.0145737](https://doi.org/10.1063/5.0145737)

Submitted: 7 February 2023 · Accepted: 6 May 2023 ·

Published Online: 24 May 2023



Shuqi Zhou (周澍祺),^{1,2} Chaoran Dou (窦超然),³ Jianzhi Li (李建志),⁴ Qiqi Zhang (张棋棋),⁵
Qilin Dai (戴其林),⁵ and Ben Xu (徐犇)^{1,2,a}

AFFILIATIONS

¹Department of Mechanical Engineering, University of Houston, Houston, Texas 77204, USA

²Department of Mechanical Engineering, Mississippi State University, Mississippi State, Mississippi 39762, USA

³Department of Industrial and Systems Engineering, Virginia Tech, Blacksburg, Virginia 24061, USA

⁴Department of Manufacturing and Industrial Engineering, The University of Texas Rio Grande Valley, Edinburg, Texas 78539, USA

⁵Department of Chemistry, Physics and Atmospheric Sciences, Jackson State University, Jackson, Mississippi 39217, USA

^aAuthor to whom correspondence should be addressed: Email: bxu12@central.uh.edu. Tel.: +1 (713) 743-5704

ABSTRACT

Laser-induced-forward-transfer (LIFT) bioprinting technology has been viewed as a regenerative medicine technology because of its high printing quality and good cell viability. To stabilize the jet to achieve high-quality printing, an energy-absorbing layer (EAL) can be introduced. In this study, three materials (graphene, gelatin, and gold) were utilized as the EAL. The effect of each EAL on the jet generation process was investigated. Besides, the effect of graphene EAL thickness was addressed for various experimental conditions. The jet generation process using sodium alginate solutions with different concentrations (1 and 2 wt. %) was also discussed to investigate the effect of viscosity. The time sequence images of the formed jets utilizing three EALs showed that both graphene EAL and gelatin EAL can promote the formation of jet flow. For the gold EAL, no jet flow was observed. This study provides experimental verifications that the interaction between laser and EAL materials can result in different jets due to various dominant interaction mechanisms. For example, strong absorption in the infrared range for the graphene EAL, strong scattering loss for the gelatin EAL, and strong absorption in the ultraviolet range but weak absorption in the infrared for the gold EAL. We also observed the holes left on the EAL after the printing was completed. The thermal effect is dominant to create regular and round shape holes for the graphene EAL, but it changes to the mechanical effect for the gold EAL because of the existence of irregular and unorganized holes. In addition, we identified the existence of an input laser energy threshold value for a certain thickness graphene EAL. More laser energy is required to break down thicker graphene EALs, which will result in a higher initial jet velocity. Furthermore, we explored the effect of sodium alginate (SA) solution's viscosity on the generated jet. We found that a high-viscosity SA solution can result in a low initial jet velocity, a short jet, and small droplets on the receiving substrate. The findings from this study help determine the mechanisms of EAL-laser interaction with different EAL materials in the LIFT process. This work aims to facilitate the development of new EAL and bioink to achieve stable jet formation and high printing quality in future LIFT bioprinting.

Published under an exclusive license by AIP Publishing. <https://doi.org/10.1063/5.0145737>

I. INTRODUCTION

Laser-induced-forward-transfer (LIFT) bioprinting, one of the laser-assisted bioprinting technologies, has drawn increasing attention in the field of regenerative medicine.^{1,2} Compared to other

bioprinting technologies, such as inkjet bioprinting and extrusion-based bioprinting, LIFT bioprinting has great advantages in high printing resolution and cell viability.³ In addition, LIFT bioprinting will not suffer from nozzle clogging, which often happens in

extrusion-based bioprinting,⁴ and it does not require high-viscosity printing materials compared with inkjet printing.^{5,6}

In the LIFT bioprinting, a laser beam passes through a focusing lens, then focuses on the bottom side of a transparent quartz (donor slide). The donor slide is coated with bioink, which is a mixture of live cells and any natural or synthetic polymers (such as hydrogels and matrigels).^{1,7} Usually, those polymers with biocompatible components and favorable properties can be used as cell-laden media. For example, hydrogel is a popular biomaterial for tissue engineering; it can be the artificial wound dressing material and the matrix for regenerating tissues or organs, so it can be a good material for cell-laden media.^{8–10} During the printing process, an f-theta lens focuses laser beams on the bottom side of the donor slide. To avoid the direct contact of the pulse laser with the bioink and enhance the energy-absorbing rate,^{11,12} an energy-absorbing layer (EAL) can be coated between the donor slide and the bioink. Once the printing process starts, the laser will irradiate the donor slide glass and then focus on the interface between the donor slide glass and the EAL. After the bioink absorbs enough laser energy, a bubble will be generated in the bioink layer. The laser-induced bubble will then expand and collapse to form a jet flow for a short period. When the jet reaches the bottom substrate, the material transfer process is completed by depositing the bioink on the receiving substrate.² The entire LIFT printing process is shown in Fig. 1.

Nevertheless, LIFT bioprinting has inevitable drawbacks due to its intrinsic working mechanism. For example, its material transfer is achieved via a jet flow; therefore, its printing quality is highly dependent on the jet regime (stable jet or unstable jet).¹³ The printing patterns for different jet regimes are shown in Fig. 2. In general, the jet flow regime is related to the rheological and mechanical properties of the bioink, as well as the laser process parameters.¹⁴ Consequently, if the jet flow regime cannot be controlled precisely, the printing quality can be low.¹⁵ On the one hand, if the developed jet is not long enough, the jet cannot reach the receiving substrate and there will be no material transfer. On the other hand, if a splashing jet or a plume jet is formed, it will print irregular and unorganized droplets on the receiving substrate, which will eventually result in low printing quality. The splashing jet can be considered the

occurrence of the side microjets or the fragments of the primary jet due to the interfacial instability, and the plume jet has many small drops breaking from the primary jet before the primary jet is formed.¹⁶ Therefore, forming a stable jet with a proper jet length is extremely critical in the LIFT bioprinting process.

Additionally, as the laser irradiates the interface between EAL and the donor slide glass, the laser beam is reflected, transmitted, and scattered. These phenomena highly depend on the selective spectral properties of EAL materials. Currently, gold (Au), silver (Ag), titanium (Ti), and some hydrogels^{17–23} have been reported as EAL materials. Their roles in the LIFT printing were believed to be evaporated due to the laser energy and generate a jet to achieve printing. It was reported that for a 50 nm thick titanium (Ti) EAL, the infrared laser (Nd:YAG) can evaporate the Ti film and lead to a jet generation process.²⁴ In some studies, gold was used as the EAL, it was found that when the laser wavelength is in the range of ultra-violet (UV) range (e.g., 355 nm), the droplet will become larger and the printing process is faster than using an infrared (IR) laser (e.g., 1064 nm).²⁵ Therefore, when the gold EAL is applied in the LIFT process, the energy transferred to generate a jet is larger from a UV laser than that from an IR laser. The differences between jet regimes of various EALs are due to the different physical properties of those EAL materials. Furthermore, it was found that EALs may break and release ruptured debris into the droplets during the LIFT process;²⁶ it is still unknown whether those metallic particles have negative impacts on cell viability.²⁷ It has been found from both *in vivo* and *in vitro* biomedical research that the micro- and nano-scale metallic particles will trigger abnormal immune responses,²⁸ which is definitely not desired in the bioprinting process. Materials with good biocompatibility may be considered a good choice as an EAL, it was reported that for some biopolymer EALs, such as Matrigel and some proteins,²⁶ the interaction between the laser and those EALs is similar to the interaction between the laser and metal EALs, so the absorbed laser energy can facilitate the local evaporation and generate a jet, but this process may need relatively high pulse laser energy (e.g., 45 μ J).^{12,29} A limited number of studies related to EAL in the LIFT process are based on inorganic non-metallic materials compared to metallic EAL. For example,

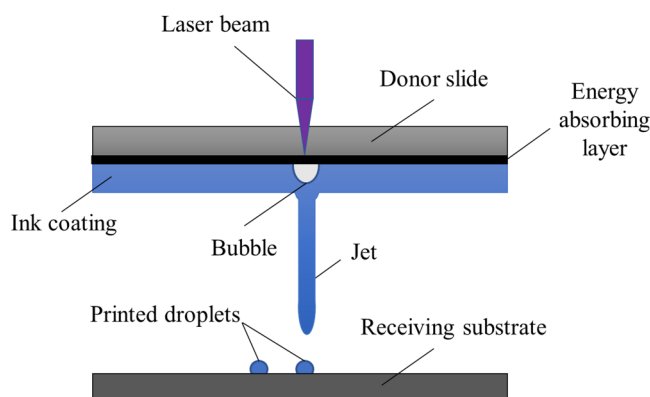


FIG. 1. Schematic of the LIFT bioprinting process.

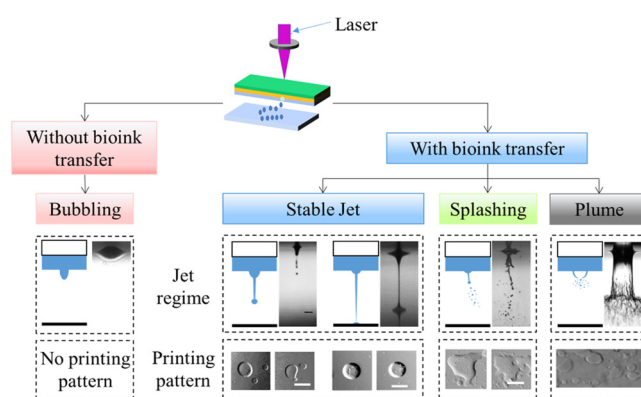


FIG. 2. Printing patterns for different jet regimes.¹⁵

graphene exhibits good biocompatibility; it has been widely used in the field of biosensors and biomedical engineering,^{30,31} and it was reported that graphene can enhance the osteogenic differentiation of hMSCs (human mesenchymal stem cells),^{32,33} which means it can play a positive role in the cultivation of certain cell lines. Therefore, graphene can be a potential material as the EAL in LIFT. Compared to other EAL materials, such as gold and gelatin, graphene may significantly improve the laser energy absorption rate, which may assist the jet generation process with certain operating parameters. Better EAL materials and designs are the keys to improving the LIFT printing quality. Therefore, evaluating the effect of different EALs on the jet regime in the LIFT process is vital to the development of the next generation of high-efficiency and high-throughput LIFT bioprinting.

Another factor influencing the quality of LIFT bioprinting is the rheology of the bioink.^{34,35} Most biological fluids and bioinks are non-Newtonian fluids,³⁶ and their strain-rate dependence and inherent viscoelasticity may lead to a different jet structure compared to Newtonian fluid jets.³⁵ The bubble dynamics in non-Newtonian fluids will be affected by the local shear stress, thus influencing the deformation of bubbles and the subsequent jet formation process. Therefore, choosing a proper viscosity of bioink plays an important role in affecting the jet formation and jet flow regime.

In this study, sodium alginate hydrogel, which is a versatile material with good biocompatibility and tailored physical properties,⁸ was utilized to coat the quartz as the bioink. It is important to note that no live cells were involved in this study since the introduction of live cells will not influence the rheology of the bioink and the jet regime during the LIFT multiphase process. In the experiment, three different materials (graphene, gold, and gelatin) were chosen as the EAL to study the effect of the EAL in the LIFT printing process, because they belong to inorganic nonmetals, organic polymers, and metals, respectively. Therefore, this study can assist to discover the benefits of adopting proper EALs for stable jets and good printing quality. The objectives of this study are (1) to demonstrate the effects of various EAL materials and the thickness of the graphene layer on the jet regime during the LIFT process and (2) to illustrate the differences in jet regimes between two sodium alginate solutions. The initial jet velocity and the size

of droplets were also measured to evaluate the printing performance. After the printing process, the EAL was observed with an optic microscope and the results were discussed.

The findings from this study will help develop new EALs for LIFT printing, facilitate the improvement of the EAL preparation process, and achieve a good printing quality while improving post-printing cell viability and survival.

II. MATERIALS AND METHODS

A. Laser printing apparatus

In this study, a customized LIFT bioprinting platform was used to conduct this experiment, as shown in Fig. 3(a). The laser generator (Spirit One 1040-8) can generate a pulse laser beam and the laser intensity follows the Gaussian distribution; the wavelength of the laser is 1040 nm, the laser spot radius is 30 μm , the pulse duration is 300 fs, and the maximum output energy is 40 μJ . During the LIFT process, several optics reflect the laser beam and lead the laser beam to pass the galvanometer. Finally, the laser beam focuses on the bottom side of the transparent quartz donor slide and then interacts with the liquid (non-EAL cases) or with the EAL (EAL cases). During this process, an XYZ stage (PRO115LM Aerotech) carries the donor slide/receiving substrate system and moves it around. The distance between the galvanometer and the donor slide was adjusted to ensure the focus of the laser beam. A high-speed camera (Phantom VEO 410L) was chosen to record the jet formation and development process. An LED light source (HL150-A Fisher Scientific) was used to provide a sharp background for the high-speed camera. In this study, the frame rate of the camera was set as 83 000 fps, which means the time interval between each frame is about 12.04 μs , and the exposure time was fixed at 10.66 μs . During the printing process, the direct writing height, which was the distance between the donor slide and the receiving slide, was fixed at 500 μm .

B. EAL preparation

To prepare the EAL and the subsequent bioink layer, ultrathin single-sided tapes (50 μm thick) were applied on the donor slide to ensure the accuracy and uniformity of the layer thickness. The

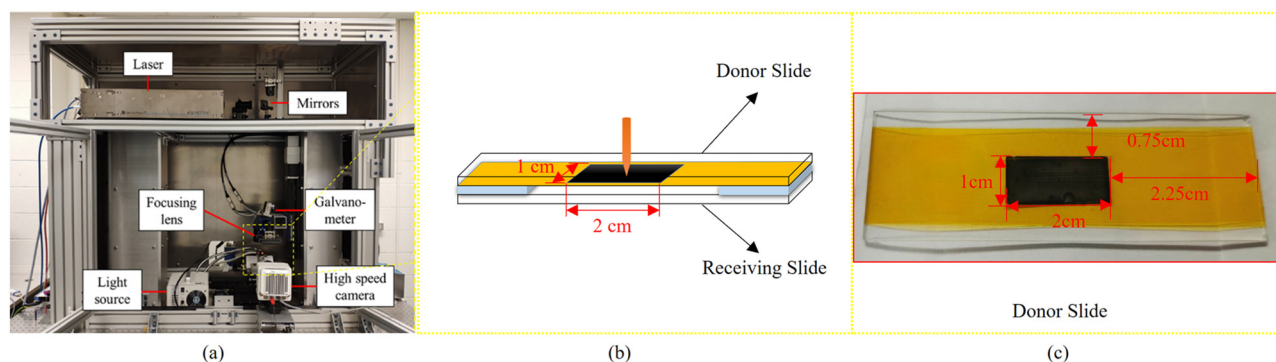


FIG. 3. (a) The LIFT experimental platform, (b) schematic of the donor ribbon structure, and (c) picture of the donor slide (with graphene EAL).

distance between the donor slide and the receiving substrate was maintained at $50\text{ }\mu\text{m}$ for single-layer tapes and $100\text{ }\mu\text{m}$ for double-layer tapes. Then, the central part of the tapes was cut out by leaving a 2 cm by 1 cm area, which was filled up with EAL material and the hydrogel bioink. As shown in Figs. 3(b) and 3(c), the ultra-thin tape is yellow, and the transparent bioink layer was coated directly on top of the EAL layer. The donor slide has a total area of 18.75 cm^2 (7.5 cm by 2.5 cm), and the coating area at the center of the quartz was 2 cm^2 (2 cm by 1 cm).

The graphene EAL was prepared by the following steps: (1) $1\text{ wt. }\%$ graphene dispersion (Sigma-Aldrich, St. Louis, MO) solution with a non-ionic surfactant Pluronic® F87 was added to the central area on the donor slide. The Pluronic® F87 surfactant is a nonionic and biocompatible polymer, and its added amount is low ($<1\text{ wt. }\%$); (2) the excess graphene solution was removed by applying the blade coating method using the edge of another slide wiping over the donor slide, so the graphene solution eventually became a smooth liquid layer by repeating this approach a few times; (3) finally, the prepared slide glasses with attached graphene solution were placed in a chamber with temperature controlled at $25\text{ }^\circ\text{C}$ overnight (about 12 h) to make sure the coated graphene solution is completely dried. After the solution evaporation was complete, the donor slides with graphene EAL were prepared. In this study, the thickness of EAL was controlled by the volume of graphene dispersion solution applied on the slides.

It is worth noting that graphene has an average diameter of less than 500 nm ; therefore, the effect of graphene on bubble generation is negligible. In addition, we assumed that there will be a negligible void between the dried graphene film and the quartz, because all the coated slide glasses were tested using mechanical forces, and no dried graphene residues were detached from the quartz. All the experiments in this study repeated the same fabrication procedure, and the results (both microscope results and jet images) are very consistent; therefore, this is another indication that there will be no significant void between the substrate and graphene film.

The corresponding volumes for thin graphene EAL and thick graphene EAL were 10 and $20\text{ }\mu\text{l}$, respectively. In this paper, we

named the thin graphene EAL as the single-layer graphene EAL and the thick graphene EAL as the double-layer graphene EAL. The thickness of the dried graphene EAL was measured by an optical microscope (Axiovert 200M), which can generate a 3D structural map for the specimen. The results show that the thickness of dried graphene EAL was about 8 and $16\text{ }\mu\text{m}$ for single-layer graphene and double-layer graphene, respectively. The detailed steps of fabricating the graphene EAL are shown in Fig. S1 in the supplementary material. Hydrogel bioink can be added later on top of the dried graphene EAL to complete the preparation of donor slides, more detail will be discussed in Sec. II C.

The gold EAL was coated in the tape-removed area using a thermal evaporation coater (MTI GSL-1700X-SPC-2), the coating process is shown in Fig. S2 in the supplementary material, and the coated gold EAL is shown in Fig. 4(a). After completing the coating, an Atomic Force Microscope (BRUKER Multimode 8) was used to measure the thickness of the gold EAL; Fig. 4(b) shows the topography image of the gold EAL in the Atomic Force Microscope (AFM). The thickness of the gold EAL is about 40 nm , similar to the values reported in other literature using the same coating approach.^{25,37}

For the gelatin EAL, type A gelatin powder (Sigma-Aldrich, St. Louis, MO) was dissolved in de-ionized water to obtain a solution with a $5\text{ wt. }\%$ concentration. Even though some literature reported that a jet can be generated using pure gelatin EAL with relatively high laser energy fluence,^{17,19,38,39} no jet formation was observed in our experiments even with the laser power tuned to its maximum. After analyzing all possible reasons, we concluded that it was because of the low absorption of laser energy. Therefore, to enhance the absorption of laser energy, black dyes were added to the gelatin solution because of their high absorptivity. Since the viscosity of the solution is much higher than the graphene dispersion solution, the coating method for graphene and gold EALs was not suitable to achieve a uniform coating; instead, a vacuum spin coater (LEBO EZ4-S) was chosen to coat the gelatin layer, as shown in Fig. S3 in the supplementary material. $2\text{ }\mu\text{l}$ gelatin solution was added to the surface of the donor slide glass, the spinning speed

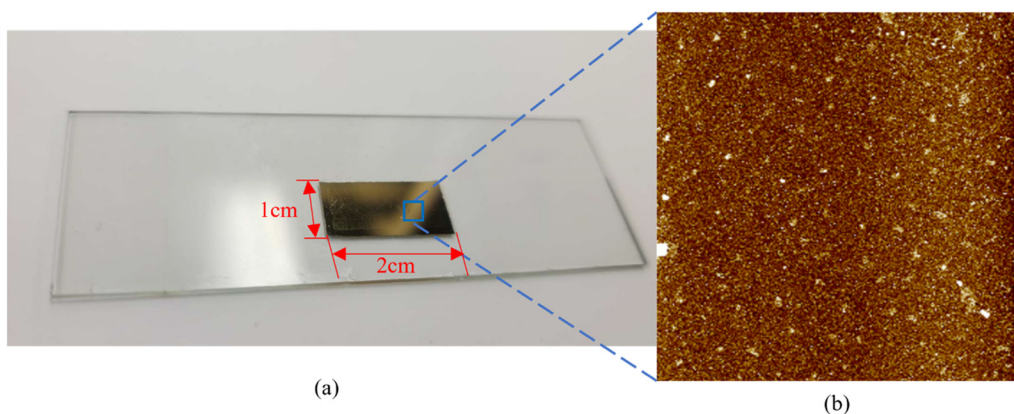


FIG. 4 (a) Picture of the gold EAL attached to donor slide and (b) topography image of gold EAL in AFM (scan area: $15 \times 15\text{ }\mu\text{m}^2$).

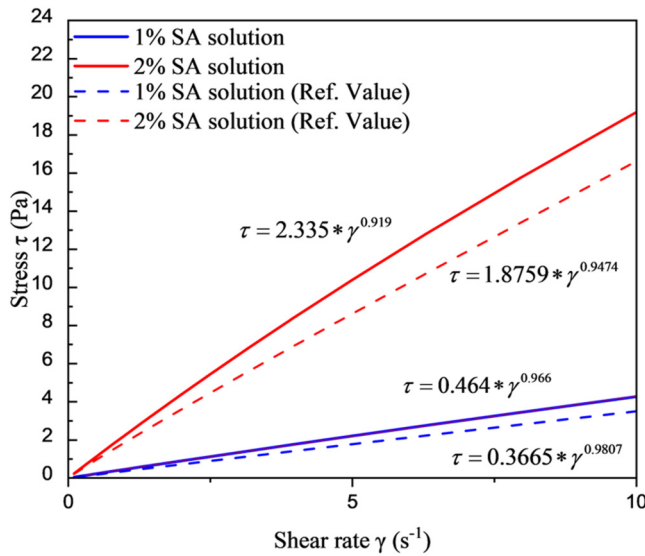


FIG. 5. Non-Newtonian behavior of 1% SA solution and 2% SA solution (the dashed lines are the curves for the same SA solution concentration in Ref. 40).

was set as 1200 rpm, and the spinning time was chosen as 20 s. The thickness of the gelatin EAL was later measured at around 10 μm .

C. Bioink/sodium alginate (SA) solution preparation

Sodium alginate powders (Sigma-Aldrich, St. Louis, MO) were dissolved in de-ionized water to prepare 1 wt. % and 2 wt. % cell-free bioinks. A rheometer (Discovery HR-2) was used to test the viscosity of both bioinks, and the results are shown in Fig. 5. When the concentration is low (1 wt. %), the bioink behaves similarly to a Newtonian fluid. However, when the concentration is high (2 wt. %), the bioink behaves like a non-Newtonian fluid, which shows a clear shear-thinning characteristic at a high shear rate. The power law model is a common rheological model to quantify non-Newtonian fluid, it can be described by the following function related to the stress and the shear rate:

$$\tau = K \cdot \gamma^n, \quad (1)$$

where τ is the stress (SI unit Pa), γ is the shear rate (SI unit s^{-1}), K is the flow consistency index (SI unit: $\text{Pa}\cdot\text{s}$), and n is the flow behavior index (dimensionless).

Based on Eq. (1), the relationship between shear rate and stress for the two SA solutions is shown in Fig. 5. It can be described by the following two power law equations:

$$\text{For 1 wt. \%SA solution: } \tau = 0.464 \cdot \gamma^{0.966}, \quad (2)$$

$$\text{For 2 wt. \%SA solution: } \tau = 2.335 \cdot \gamma^{0.919}, \quad (3)$$

where the flow consistency indexes are 0.464 and 2.335 Pa s, and

the flow behavior indexes are 0.966 and 0.919 for 1 and 2 wt. % SA solutions, respectively.

Ahn *et al.*⁴⁰ reported the non-Newtonian flow behavior for similar SA solutions, and their results are also plotted in Fig. 5. It can be concluded that the fitted curves from our experiments match well with the reference results from them, and it also verifies that the SA solution used in this study is a shear-thinning fluid.

After preparing the SA solutions, they were coated on top of the EAL. For the SA hydrogel coating on the graphene EAL and the gold EAL, the coating steps areas can be found in Fig. S4 in the supplementary material: (1) To ensure enough space for coating 100 μm SA hydrogel, another two layers of ultrathin single-sided tapes (100 μm in thickness) with the central area removed were prepared. The removed area was slightly smaller than the area of graphene EAL (about $1.9 \times 0.9 \text{ cm}^2$); (2) the prepared tapes were attached to the slide, and the removed area was over the EAL coating area, which can provide a fixed space for the subsequent SA hydrogel coating; (3) using the same method for graphene EAL coating described in Sec. II B, the SA hydrogel was coated on top of the EAL layer. It is worth noting that the volume of SA hydrogel added was 20 μl .

Due to the high viscosity of the SA solution, the spin coating method was also adopted to coat the SA hydrogel on top of the gelatin EAL, as shown in Fig. S5 in the supplementary material. In the experiment, 20 μl SA hydrogel was added into the central area, the spinning speed was set as 1200 rpm, and the spinning time was chosen as 20 s. Since no significant removal of SA hydrogel was observed and they were confined within the area surrounded by the ultrathin tapes, the layer thickness of coated SA hydrogel maintained the same 100 μm thickness as that of two layers of ultrathin tapes.

D. Design of experiments (DOE)

The DOE was summarized in Table I. By comparing the results between cases with EAL and without EAL, the effect of corresponding EAL on the jet regime can be investigated. For graphene EAL, the effect of EAL thickness was also explored. To investigate the effect of bioink viscosity on the jet formation process, 1 wt. % SA solution and 2 wt. % SA solution were printed. In all experiments, the volume of the SA solution was 20 μl ; this ensured a relatively constant bioink layer thickness of 100 μm . The distance between the donor slide and the receiving substrate was fixed as 500 μm by attaching 10 layers of ultrathin tape (50 μm thickness for each layer) at both right and left ends of the receiving substrate surface.

E. Data analysis

After the experiment, statistical analysis was performed to compare those cases, three samples from each group were used as the original data, and the quantitative value shown in the results was based on mean value \pm standard deviation. The standard deviation was calculated using Eq. (4),

$$s = \sqrt{\frac{\sum (x_i - \mu)^2}{N - 1}}, \quad (4)$$

TABLE I. Design of experiments.

Liquid layer material	EAL	Laser fluence (mJ/cm ² , each increase of 566 mJ/cm ²)	Corresponding laser pulse energy (μJ, each increase of 4 mJ/cm ²)
1% SA solution	No	2260–5660	16–40
	Graphene (single layer)	2260–5660	16–40
	Graphene (double layers)	2260–5660	16–40
	Gold	2260–5660	16–40
	Gelatin	2260–5660	16–40
2% SA solution	No	2260–5660	16–40
	Graphene (single layer)	2260–5660	16–40
	Graphene (double layers)	2260–5660	16–40
	Gold	2260–5660	16–40
	Gelatin	2260–5660	16–40

where s is the standard deviation, N is the size of samples, x_i is each value from the samples, and μ is the mean value of the samples.

The Statistically Significant Difference (SSD) between the data of the two groups was calculated using the two-sample t-test method, and the test statistic is calculated in Eq. (5),

$$t = \frac{(x_1 - x_2)}{s_p \sqrt{1/N_1 + 1/N_2}}, \quad (5)$$

where t is the test statistic, x_i is the mean value from samples, N is the size of samples, and s_p is the pooled variance.

s_p can be calculated using Eq. (6),

$$s_p^2 = \frac{((N_1 - 1)s_1^2) + ((N_2 - 1)s_2^2)}{N_1 + N_2 - 2}. \quad (6)$$

A 95% confidence interval was used in this study and the α -value was 0.05.

III. RESULTS AND DISCUSSIONS

A. Effect of EAL on the jet formation

To compare the effects of various types of EALs on the formation of laser-induced jets, the generated jets captured by the high-speed camera during the printing process were compared and characterized in this section. The time sequence images of induced

jets for both 1 and 2 wt. % SA solutions without EAL are shown in Fig. 6, and the jet images for different graphene EAL thicknesses are shown in Figs. 7 and 8. Finally, the jets generated from 1 wt. % SA solution with gold EAL and gelatin EAL are shown in Fig. 9.

When the donor slides were not coated with any EAL materials, as shown in Fig. 6, the time sequence images show that no jets were generated even with the maximum laser power (40 μJ per pulse), according to the time sequence images. This was mainly because the bubbles were not fully formed in the SA layer due to the low laser energy absorption rate of SA. Figure 6(a) shows that the liquid layer close to the donor slide had only minor deformation due to the bubble expansion in the 1 wt. % SA. Such a shape deformation could not be observed in the 2 wt. % SA, since it would require an even higher laser energy input. Due to the lack of enough laser energy input, a jet flow could not be generated for a complete hydrogel transfer process.

However, when graphene EALs were applied for the same 1 wt. % SA hydrogel, a stable jet can be formed even when the laser pulse energy was as low as 16 μJ. As shown in Figs. 7(a) and 7(d), stable jets were generated for both single-layer and double-layer graphene EAL. Therefore, it can be concluded that the graphene EAL helped absorb more thermal energy from the laser because the graphene EAL has a dark color to absorb more thermal energy in the infrared range (1040 nm wavelength). In other words, the graphene EAL assisted to reduce the required laser energy input so that a stable jet can be generated. We can also observe that a

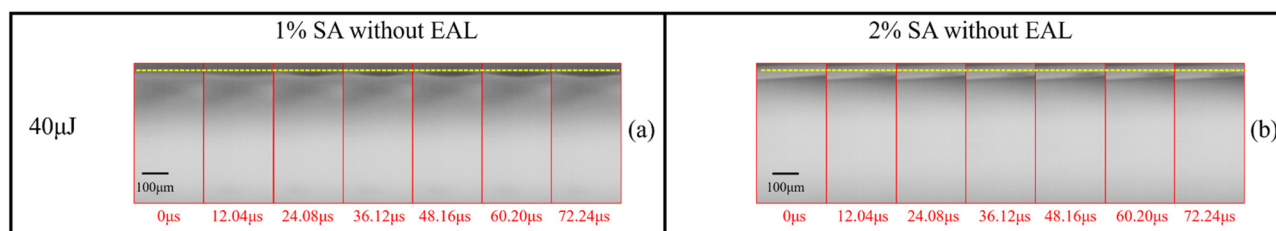


FIG. 6. The time sequence images of the LIFT printing process without EAL for (a) 1% SA solution and (b) 2% SA solution (yellow dashed lines are the jet generation position).

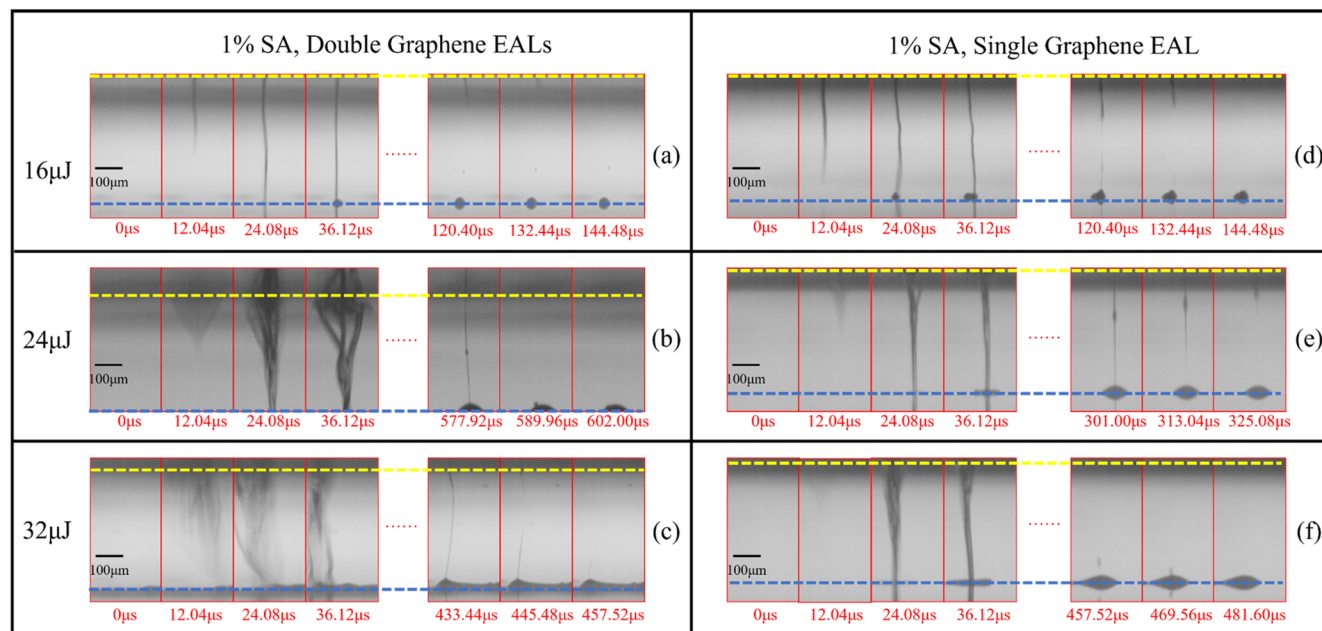


FIG. 7. The generation of jets during the LIFT process using graphene EAL for 1% SA hydrogel (yellow dashed lines are the jet generation position, and blue dashed lines are the receiving slide position).

complete jet existed at $120.4\mu\text{s}$ for the single-layer graphene EAL. At the same time, for the double-layer graphene EAL, no complete jet was observed; this is because more laser energy was required to maintain a stable jet compared to a single-layer graphene EAL; therefore, a stable jet could not last very long for the double-layer graphene EAL.

Figure 7 also demonstrates that when the laser energy was increased to 24 and $32\mu\text{J}$, jets became unstable for double-layer graphene EAL, as shown in Figs. 7(b) and 7(c), and the corresponding jet regimes belonged to the splashing jets (as explained in Fig. 2). Apparently, such jet modes cannot transfer the liquid to the receiving slide with organized patterns. Nevertheless, the same levels of laser energy can generate stable jets for single-layer graphene EAL, as shown in Figs. 7(e) and 7(f). The width of jets was gradually reduced over time, and it means that most of the liquid transfer was completed at the early stage of the LIFT printing. An interesting phenomenon that can be found in Figs. 7(b) and 7(c) is that the splashing jets eventually became much narrower after at least $400\mu\text{s}$, but they were not considered stable jets because they cannot successfully transfer the SA hydrogel from the donor slide to the receiving slide.

The effects of graphene EALs on the jet formation using 2 wt. % SA solution can be found in Fig. 8. When the laser energy was $24\mu\text{J}$ for a double-layer graphene EAL, no complete jet was created. Minor deformations of the SA hydrogel layer can be observed right below the yellow dashed line in Fig. 8(a), and the minor deformation is probably due to the formation of small bubbles in the SA layer. Such a deformation gradually disappeared after $36\mu\text{s}$, and this indicates that the input laser energy was not

large enough to induce the formation of a jet. Situations became different when single-layer graphene EAL was adopted; for the same level of laser energy ($24\mu\text{J}$), as shown in Fig. 8(d), a jet was formed around $12\mu\text{s}$. However, such a jet quickly bounced back to the donor slide after $24.08\mu\text{s}$, and a complete jet transfer was not achieved by reaching the bottom receiving substrate. A very likely reason was that the input laser energy was not high enough to overcome the stronger surface tension of 2 wt. % SA solution and achieve the full development of jets. Consequently, once the laser energy was increased to $32\mu\text{J}$ for both cases, a stable jet was formed to transfer the SA solution to the receiving slide, as shown in Figs. 8(b) and 8(e). When the input laser energy was further increased to $36\mu\text{J}$, a complete jet transfer can still be observed. However, the jet width was larger than that with a lower laser energy, and the transfer process was not extended significantly when compared Figs. 8(b), 8(c), 8(e), and 8(f). Similar to the cases with 1% SA solution (Fig. 7), the existence of graphene EAL in 2% SA hydrogel also promotes the generation of jet due to the high absorption of graphene.

Finally, Fig. 8(c) demonstrates an interesting observation that during the post-stage of printing (after $927\mu\text{s}$), a small drop was observed just above the major drop. The small drop fell on top of the major drop and eventually merged with the remaining drop on the receiver slide. This is a special phenomenon in viscoelastic fluids, and it only occurs when the fluid experiences the capillary thinning effect. The sinusoidal instability along the surface of the thin fluid thread and the successive contractions and relaxation along with the interface of the thread will lead to a pattern of small drops.^{41,42} It was also reported that this phenomenon was partially

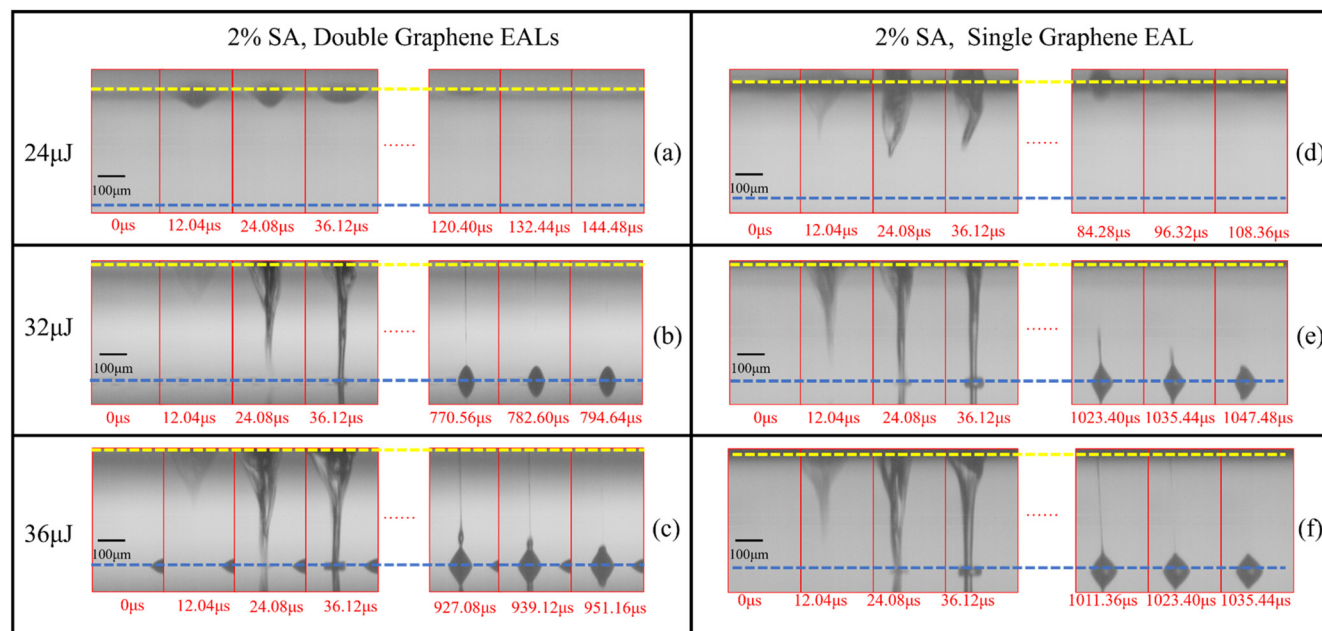


FIG. 8. The generation of jets during the LIFT process using graphene EAL for 2% SA hydrogel.

related to the high jet speed.⁴³ The jet velocity might have been large in the beginning stage of our experiment (unfortunately it is extremely hard to record the initial jet speed), and this also indicates that more energy was transferred into the SA hydrogel at the beginning stage of LIFT printing due to the application of double-layer graphene EAL.

Figure 9 shows the comparison between gold EAL and gelatin EAL when 1 wt. % SA and 2 wt. % SA solution was used. When the gold EAL was applied for 1 wt. % SA solution cases, no jet can be observed even when the laser energy was as high as 40 μ J, as shown in Figs. 9(a) and 9(b). However, in 1 wt. % SA cases, with the application of gelatin EAL, a short jet (maximum length 108.6 μ m) can be observed when the laser input energy was 40 μ J from Fig. 9(d). No jet was formed when the laser input energy was 32 μ J. A similar phenomenon can be found when using 2 wt. % SA solution, as shown in Figs. 9(g) and 9(h). When the laser energy was 32 μ J, negligible bubble can be observed near the bottom boundary of SA layer, but a larger bubble can be observed when applying 40 μ J laser energy. Unfortunately, no formed jet could reach the receiving slide. For cases with 2 wt. % SA using gold EAL, they can be found in Figs. 9(c) and 9(f), apparently similarly as in Figs. 9(a) and 9(b) no bubble or jet can be formed. When comparing these cases, adopting gelatin EAL can assist the formation of jet flow, but the formed jet was not long enough to transfer the SA hydrogel from the donor slide to the receiving slide even if the highest laser energy was chosen. We also found in Figs. 9(a), 9(b), 9(c), and 9(f) that a cluster of bright spots appeared on the top portion, and the number of bright spots increased with the increase in laser energy. This phenomenon may attribute to the gold ablation caused by

focusing laser energy, thus resulting in visible plasma in a very short time period.^{44,45}

To summarize the study in this section, different performances of jet/bubble formation were observed when various EALs were adopted; such differences may be due to the interactions between laser and EALs. For graphene EAL, the absorption efficiency is relatively high, which means that more laser energy can be absorbed to generate a bubble leading to jet formation. On the contrary, gold has a relatively high reflection rate when the laser wavelength is above 630 nm. For example, when the laser wavelength is 1060 nm, the reflection rate is about 92%.⁴⁵ The results in this study related to the gold EAL can verify the findings from Koch *et al.*²⁵ This means the absorbed laser energy when gold EAL is chosen should be much lower than that of graphene EAL cases. As for the gelatin EAL, though black dye was added to improve the energy absorption rate, the formed jet is much shorter (108.6 μ m) than that in graphene EAL cases. A shorter jet means that the laser energy for jet generation is much lower than that in graphene EAL cases because gelatin is a polymer gel and its scatter rate is relatively high.⁴⁶ Therefore, when gelatin was used as the EAL material, the scattering loss may account for most of the absorbed laser energy; that is also the reason why with the same laser energy input the jet length in the gelatin case was much shorter.

B. Comparison of the impact holes on the donor slide between graphene EAL and gold EAL

After the contact between the pulse laser and the donor slide, holes were left over on the EALs due to thermal effect and/or

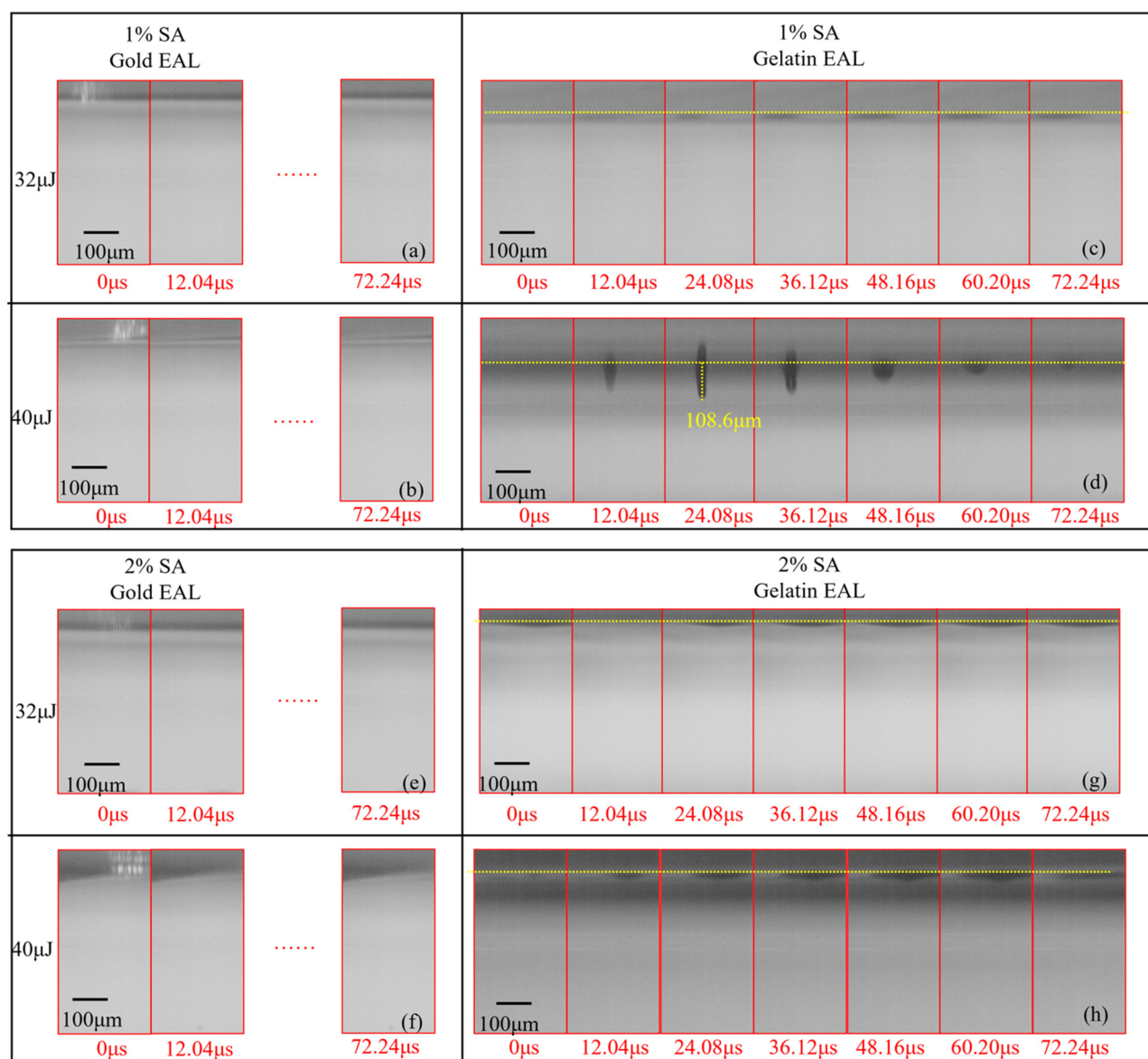


FIG. 9. Images of the LIFT process for 1% and 2% SA with gold EAL at different laser energy.

mechanical impact, as shown in Fig. 10. It is critical to note that after the LIFT printing using the gelatin EAL, the SA hydrogel filled in the holes. It was difficult to observe the damage of EAL through an optic microscope, so the gelatin EAL was not chosen to be characterized using an optical microscope. Based on the measured hole sizes, a quantitative comparison of the maximum hole size at two levels of pulse energies between the graphene EAL and the gold EAL is shown in Fig. 11.

At a lower pulse laser energy level, there was a great difference in hole sizes between the graphene EAL and the gold EAL. This is

because the input laser energy was mostly reflected by the gold EAL, but the graphene EAL had a decent energy-absorbing capability due to its high absorptivity in the infrared range. When the laser energy was increased from 16 to 32 μJ , the holes on the gold EAL had a very similar hole size (less than 10% difference) compared to the ones on the graphene EAL, as shown in Figs. 10 and 11. We can also analyze the relative increase in hole sizes for each case, and it turned out that the corresponding increment was 14.34%, 31.97%, and 298.52% for the single-layer graphene EAL, the double-layer graphene EAL, and the gold EAL, respectively.

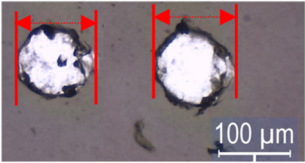
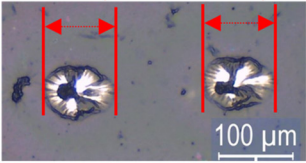
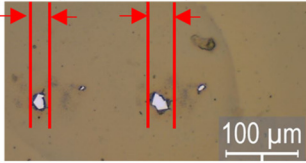
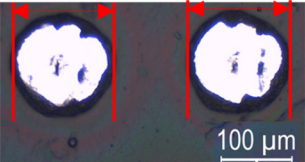
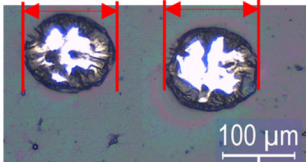
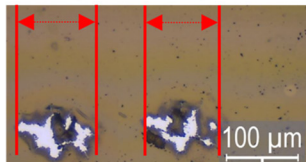
Laser Energy	Single Graphene EAL	Double Graphene EAL	Gold EAL
16 μ J	 <p>(a)</p>	 <p>(b)</p>	 <p>(c)</p>
32 μ J	 <p>(d)</p>	 <p>(e)</p>	 <p>(f)</p>

FIG. 10. Microscope images of holes on graphene EAL and gold EAL after LIFT printing (Bioink: 1 wt. % SA).

The sizes of holes increased significantly for the gold EAL, but the increase for graphene EALs was relatively smaller. The single-layer graphene EAL had a less than 50% increase compared to double-layer graphene EAL. This indicates that the capability of absorbing energy from the UV range was enhanced when the input laser energy was increased causing the mechanical impacts to be more dominant than the thermal effects; this can easily be observed from

Figs. 10(c) and 10(f) because of the existence of uneven edges with irregular shapes on the gold EAL, and they were not like the round shape in Figs. 10(a), 10(b), 10(d), and 10(e).

In addition, irregular graphene pieces can be found in Figs. 10(b), (a), (c), and (e) inside a round edge due to the thermal effect of the double-layer graphene EAL. In addition, it can be found that the edge of single-layer EAL hole is more uniform, while the holes in the double-layer EAL had irregular shapes. It is important to note that these irregular pieces were not caused by the mechanical impact of the pulse laser. Instead, they remained inside the round edge because of the adoption of double-layer graphene, which would require higher laser energy to fully “burn” (remove) the leftover pieces (dried graphene residuals). This would influence the induced jet regime by forming a splashing jet, as shown in Fig. 7(c), and more comparisons between the single-layer graphene EAL case and double-layer EAL case will be discussed in Sec. III C. For the gold EAL, it can be concluded from Figs. 9(a) and 9(b) that even when the laser energy was as high as 40 μ J (maximum laser energy on the laser generator), there was still no jet formed. The possible mechanical impact affected the uneven and irregular edges of the gold EAL, which simultaneously influenced the jet formation. Because of this, it is critical to properly tune the laser input energy to form a stable jet and improve the printing quality.

C. Effect of the graphene EAL thickness on the jet generation

From the discussions in Sec. III A, adopting the graphene EAL shows great potential to assist in generating stable jets with reduced laser input energy. Moreover, the thickness of the graphene EAL plays an important role in determining the initial jet velocity.

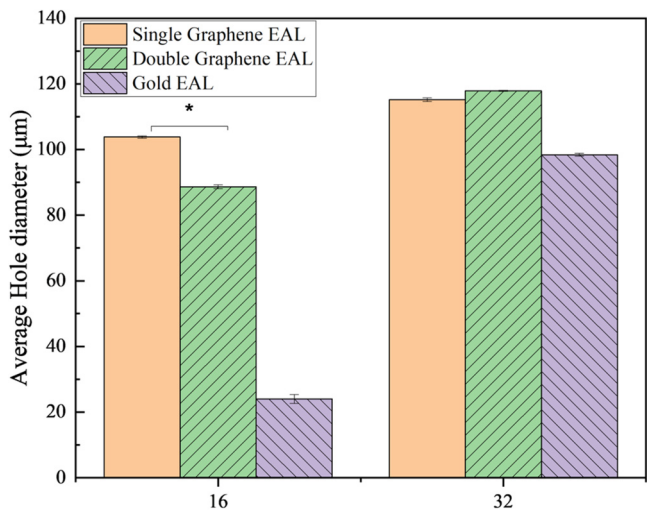


FIG. 11. Diameter of the hole in different EALs [error bars represent a plus/minus one standard deviation, and asterisk (*) indicates the significant difference between groups].

In this section, the effects of graphene EAL thickness on jet initial velocity will be discussed.

It was reported that the jet velocity greatly influences the process-induced cell injury during the LIFT printing because higher jet velocity can cause mechanical impacts between the cell-laden bioink and the receiving substrate during the landing.³⁸ It is expected that the thickness of EAL can control the initial jet velocity to avoid a very high initial speed.³⁹ To assess such a hypothesis, in this study the jet velocity was calculated based on the time difference between the first two image frames as well as the distance where the jet traveled. The results are shown in Fig. 12(a). When the 1 wt. % SA hydrogel was chosen and the laser energy was low (24 μ J), the initial jet velocity from the thicker EAL (15 μ m) case was 17.53 m/s; it became 22.94 m/s for thinner EAL (8 μ m) case. Therefore, higher initial jet velocity requires higher absorbed energy if the input laser energy is the same, for a thinner graphene EAL the transferred energy to generate a jet should be higher than that in a thicker graphene EAL when the input laser energy was 24 μ J. In other words, when a thicker EAL was adopted, the energy required to regenerate a jet was higher than that with a thinner EAL. Nevertheless, when the laser input energy was increased to 28 and 32 μ J, thicker EAL always could generate faster initial jet velocity. For example, a double-layer graphene EAL formed a jet velocity as high as 31.5 m/s, but such an initial jet velocity was reduced to 26.79 m/s when single-layer graphene EAL was adopted and 32 μ J laser pulse energy was utilized. Therefore, it is expected that there is a threshold value for input laser energy between 24 and 28 μ J. Thicker EALs can generate faster initial jet velocity when the laser energy is above the threshold. Such an observation is

consistent with the hypothesis discussed in Sec. III B: with a thicker EAL, higher input laser energy was required to fully burn the EAL. Once the EAL was fully burned, more energy was accumulated around the irradiated area inside the thick EAL, and more energy was then transferred to generate a jet, thus resulting in a higher initial jet velocity.

However, when 2 wt. % SA solution was used, the conclusions are different because thinner EAL always generated faster initial jet velocity than the thicker EAL cases. This difference attributes from the effect of viscosity, and more details will be discussed in Sec. III D.

Since the accuracy of bioprinting highly depends on the droplet size,⁴⁷ the sizes of droplets for various thicknesses of graphene EAL were investigated in this study, as shown in Fig. 12(b). For both SA solutions (1 and 2 wt. %), the droplet size was reduced with the application of double-layer graphene EAL, and the size reduction was up to 32.53% for 1% SA when 32 μ J laser energy was used. On the other hand, compared with jet images in Figs. 7(c) and 7(f), when 32 μ J laser energy was chosen, the jet tends to splash when single-layer graphene EALs were adopted. This may lead to a quite irregular printing pattern and cause low printing quality eventually. However, with the application of double-layer graphene EALs, the jet became more stable. So a proper increase in the graphene EAL thickness can help improve the printing quality and the cell viability. There is no doubt that those findings can help determine the optimal EAL thickness for LIFT bioprinting.

Finally, the thicknesses of single-layer and double-layer graphene EALs were measured after the printing, and the test results showed that the average thickness was reduced from 10 to about

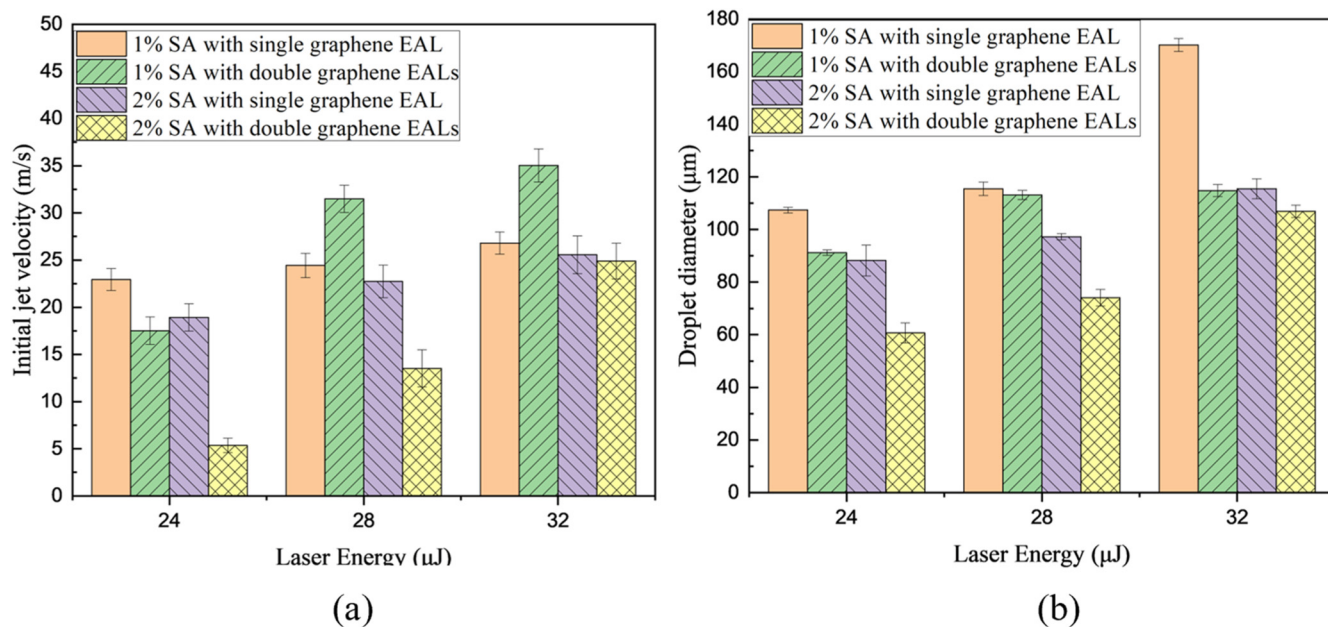


FIG. 12. (a) Initial jet velocity and (b) droplet diameter in different cases (error bars represent a plus/minus one standard deviation).

$8\mu\text{m}$ for single-layer graphene EAL at the laser irradiation point, and from 20 to about $15\mu\text{m}$ for double-layer graphene EAL at the laser irradiation point. Most of the lost graphene went to the receiving substrate together with the jet flow in the transfer process, but some of them may be burned out due to the thermal effects from the absorbed laser energy.

D. Effect of the viscosity of SA bioink on the jet generation

From the rheological test results shown in Fig. 5, the dynamic viscosity of the 2 wt. % SA solution was around 2.321 Pa S, and the dynamic viscosity of 1 wt. % SA solution was about 0.473 Pa S. By comparing Figs. 7(d) and 8(d), it can be found that when the input laser energy was maintained the same ($24\mu\text{J}$), no jet could reach the receiving substrate using 2 wt. % SA bioink with a single-layer graphene EAL. A stable jet with proper length reached the receiving slide when 1 wt. % SA bioink with a single-layer graphene EAL was adopted. As discussed in Sec. III C, a quantitative analysis for the initial jet velocity was shown in Fig. 12(a) for four different cases, including 2 wt. % SA solutions. It can be found that when using the 2 wt. % SA as the bioink with double-layer EAL and maintaining $28\mu\text{J}$ input laser energy, the initial jet velocity was 13.52 m/s, which was only 42.92% of the initial jet velocity for the case of 1 wt. % SA solution. This implies that lower initial jet velocity means less absorbed laser energy by the SA solution. Therefore, for high-viscosity fluids, greater laser energy is required to generate a stable jet and transfer the SA solution to the receiving substrate; this may challenge the printability and the required laser input energy, because high-viscosity fluids may have a greater viscous

dissipation rate than that of low viscosity fluids possibly leading to a lower jet velocity and low-quality printing.

As discussed in Sec. III C, there is a threshold laser energy between 24 and $28\mu\text{J}$ to trigger a stable jet flow for double-layer EALs. A hypothesis naturally arises here based on the experimental discoveries: the threshold laser energy for high viscous fluids is larger than that of low viscous fluids. It can be found in Fig. 12(a) that for 2 wt. % SA bioink when the laser energy was increased from 28 to $32\mu\text{J}$, the relative difference of initial jet velocity for a double-layer EAL was 54.59%, which is greater than that of a single-layer EAL (11.24%). We can then predict that when the input laser energy keeps increasing, the initial jet velocity of a thick EAL (e.g., double-layer) will eventually exceed that of a thin EAL (e.g., single-layer), no matter what weight percentage of the SA solution is. Such a prediction is also consistent with what has been discussed in Secs. III B and III C: (a) when applying sufficient input laser energy, it can burn the graphene EAL in a local area; (b) high initial jet velocity can be achieved by using thicker graphene EAL, so more energy can be transferred through such a thick EAL.

Furthermore, since the thermal conductivity is higher than that of 1% SA solution for 2 wt. % SA solution,⁴⁸ less laser energy can be involved in the “burning” process due to the interaction between the laser beam and the graphene EAL; this, in turn, resulted in a higher required input laser energy to complete the liquid transfer process while maintaining the “burning” in a local region.

Figure 13 shows the time sequence jet images at $28\mu\text{J}$ input laser energy for 1 and 2 wt% SA solutions. It can be found that once the droplet was completely detached from the jet and landed

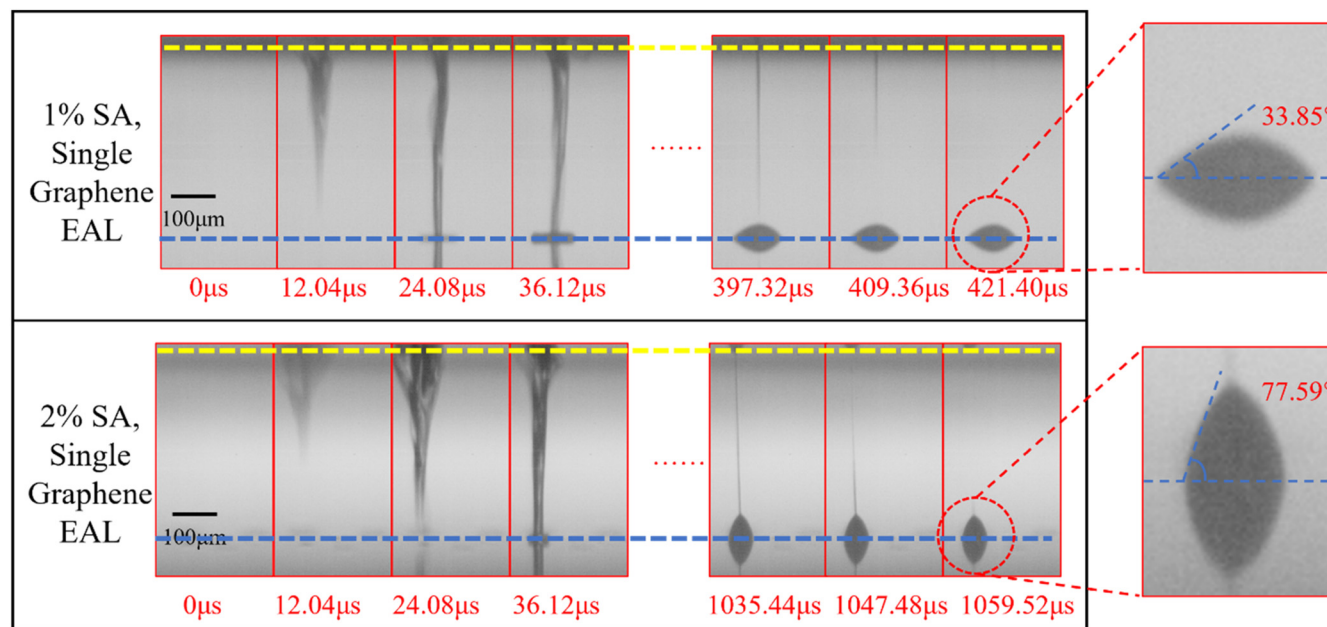


FIG. 13. The generation of jet for two SA solutions with single-layer graphene EAL at $28\mu\text{J}$ input laser energy.

on the receiving substrate, the droplet contact angle for 2 wt. % SA was 77.59°, which is almost two times larger than that of 1 wt. % SA. Such a difference is due to the viscosity of the two SA solutions. More viscous SA possesses a larger droplet contact angle on the receiving substrate. The difference in viscosity may further influence the jet developing time. For instance, once the jet lands on the receiving slide, the detached droplet will expand due to the remaining momentum and gravity. The bottom side of the jet may then merge with the droplet, but its top side will experience a strong upward tension due to the viscoelasticity of the SA solution. Therefore, for fluid with higher viscosity, this process may take a longer time. Such a phenomenon will affect the volume of landed droplets and the jet developing time. Many factors play important roles in determining this process, such as the physical properties of SA, the thickness of EAL, the jet width, and the jet velocity when touching the receiving substrate. As shown in Fig. 13, even though the jet reached the receiving substrate at almost the same time for both 1 and 2 wt% SA solutions, it took a much longer time for the fluid with a higher viscosity (2 wt. % SA) to detach from the primary jet. In the end, it took 1059.52 μ s for 2 wt. % SA solution to complete the printing process, but 1 wt. % SA solution only took 421.4 μ s.

IV. CONCLUSIONS

The quality of LIFT printing is highly dependent on the stability of the jet flow, and it is determined by operating parameters (e.g., input laser energy, viscosity of bioink, EAL materials, and EAL thickness). In this study, we investigated three different materials (graphene, gold, and gelatin) as the EAL material and evaluated their effects on jet regimes, several major conclusions can be drawn from this study:

- (1) The analysis of post-printing hole sizes on the EAL reveals that the thermal effect is dominant in creating a regular round shape hole for the graphene EAL. For the gold EAL, the mechanical effect is the most important factor because of the existence of irregular and unorganized holes.
- (2) The thickness of graphene EAL influences the jet formation process, and the input laser energy needs to be greater than a threshold to get fully broken down for a specific thickness graphene EAL. For example, thicker graphene EAL requires more laser energy to be fully burned, which can also transfer more laser energy to generate a jet with a higher initial velocity. Otherwise, the generated jet will be shorter than that of a thinner graphene EAL case with the same input laser energy.
- (3) The viscosity of the SA solution also plays an important role in the jet formation mainly because of the high dissipation rate of high-viscosity fluid by reducing the energy for jet generation during LIFT. For example, the high-viscosity SA solution will result in a low initial jet velocity, a short jet, and small droplets on the receiving substrate.

The findings in this study can help researchers better understand the role of EAL in the LIFT process and the importance of bioink rheology. The goal of our work is to facilitate the development of new EAL and bioink. More specifically, optimizing the EAL design and the physical properties of bioink is critical to

reduce the potential risk of cell death due to mechanical forces and achieving high-quality printing in future cell-laden LIFT printing.

SUPPLEMENTARY MATERIAL

See the supplementary material for the preparation process of graphene EAL, gold EAL, and gelatin EAL, as well as the SA coating process on these EALs.

ACKNOWLEDGMENTS

The authors are grateful for the funding support from the Presidential Frontier Faculty Fellow Program at University of Houston and the student support from Mississippi State University. We also appreciate part of the equipment support from the U.S. Department of Defense Manufacturing Engineering Education Program (MEEP) program under Award No. N00014-19-1-2728. We thank Dr. Kundu Santanu in the School of Chemical Engineering at Mississippi State University for providing the viscometer to measure the viscosity of SA solutions, and we are also grateful for the help from Dr. Kun Wang and his PhD student Mr. Haixin Zhang in the School of Physics and Chemistry at Mississippi State University to measure the thickness of the gold EAL using AFM.

AUTHOR DECLARATIONS

Conflict of Interest

The authors have no conflicts to disclose.

Author Contributions

Shuqi Zhou: Data curation (equal); Formal analysis (equal); Investigation (equal); Methodology (equal); Writing – original draft (lead); Writing – review & editing (equal). **Chaoran Dou:** Data curation (equal); Formal analysis (equal); Investigation (equal); Methodology (equal); Writing – review & editing (supporting). **Jianzhi Li:** Funding acquisition (equal); Investigation (equal); Methodology (equal); Project administration (equal); Resources (equal); Writing – review & editing (supporting). **Qiqi Zhang:** Formal analysis (supporting); Investigation (supporting); Resources (supporting). **Qilin Dai:** Resources (equal); Writing – review & editing (supporting). **Ben Xu:** Conceptualization (lead); Data curation (equal); Formal analysis (equal); Funding acquisition (lead); Investigation (equal); Methodology (equal); Project administration (lead); Resources (equal); Supervision (lead); Writing – review & editing (lead).

DATA AVAILABILITY

The data that support the findings of this study are available within the article.

REFERENCES

- ¹A. A. Antoshin *et al.*, “LIFT-bioprinting, is it worth it?,” *Bioprinting* **15**, e00052 (2019).
- ²C. Dou *et al.*, “A state-of-the-art review of laser-assisted bioprinting and its future research trends,” *ChemBioEng Rev.* **8**, 517–534 (2021).

- ³L. Koch *et al.*, "Laser printing of skin cells and human stem cells," *Tissue Eng., Part C* **16**, 847–854 (2010).
- ⁴M. Morales, D. Munoz-Martin, A. Marquez, S. Lauzurica, and C. Molpeceres, "Laser-induced forward transfer techniques and applications," in *Advances in Laser Materials Processing: Technology, Research and Applications* (Elsevier Ltd., 2017).
- ⁵M. V. Gorlenko *et al.*, "Laser microsampling of soil microbial community," *J. Biol. Eng.* **12**, 1–11 (2018).
- ⁶V. I. Yusupov, M. V. Gorlenko, V. S. Cheptsov, N. V. Minaev, E. S. Churbanova, V. S. Zhigarkov, E. A. Chutko, S. A. Evlashin, B. N. Chichkov, and V. N. Bagratashvili, "Laser engineering of microbial systems," *Laser Phys. Lett.* **15**(6), 065604 (2018).
- ⁷R. K. Pirlo, P. Wu, J. Liu, and B. Ringeisen, "PLGA/hydrogel biopapers as a stackable substrate for printing HUVEC networks via BioLPTM," *Biotechnol. Bioeng.* **109**, 262–273 (2012).
- ⁸A. S. Hoffman, "Hydrogels for biomedical applications," *Adv. Drug Delivery Rev.* **64**, 18–23 (2012).
- ⁹S. V. Murphy and A. Atala, "3D bioprinting of tissues and organs," *Nat. Biotechnol.* **32**, 773–785 (2014).
- ¹⁰M. L. Oyen, "Mechanical characterisation of hydrogel materials," *Int. Mater. Rev.* **59**, 44–59 (2014).
- ¹¹B. Hopp *et al.*, "Survival and proliferative ability of various living cell types after laser-induced forward transfer," *Tissue Eng.* **11**, 1817–1823 (2005).
- ¹²N. T. Kattamis, N. D. McDaniel, S. Bernhard, and C. B. Arnold, "Laser direct write printing of sensitive and robust light emitting organic molecules," *Appl. Phys. Lett.* **94**, 103306 (2009).
- ¹³B. Guillotin *et al.*, "Laser assisted bioprinting of engineered tissue with high cell density and microscale organization," *Biomaterials* **31**, 7250–7256 (2010).
- ¹⁴Z. Zhang, R. Xiong, R. Mei, Y. Huang, and D. B. Chrisey, "Time-resolved imaging study of jetting dynamics during laser printing of viscoelastic alginate solutions," *Langmuir* **31**, 6447–6456 (2015).
- ¹⁵J. Qu *et al.*, "Printing quality improvement for laser-induced forward transfer bioprinting: Numerical modeling and experimental validation," *Phys. Fluids* **33**, 071906 (2021).
- ¹⁶M. Jalaal, S. Li, M. Klein Schaarsberg, Y. Qin, and D. Lohse, "Destructive mechanisms in laser induced forward transfer," *Appl. Phys. Lett.* **114**, 213703 (2019).
- ¹⁷A. D. Dias, A. M. Unser, Y. Xie, D. B. Chrisey, and D. T. Corr, "Generating size-controlled embryoid bodies using laser direct-write," *Biofabrication* **6**, 025007 (2014).
- ¹⁸M. Gruene *et al.*, "Laser printing of three-dimensional multicellular arrays for studies of cell-cell and cell-environment interactions," *Tissue Eng., Part C* **17**, 973–982 (2011).
- ¹⁹D. M. Kingsley, A. D. Dias, D. B. Chrisey, and D. T. Corr, "Single-step laser-based fabrication and patterning of cell-encapsulated alginate microbeads," *Biofabrication* **5**, 045006 (2013).
- ²⁰L. Koch *et al.*, "Laser bioprinting of human induced pluripotent stem cells—The effect of printing and biomaterials on cell survival, pluripotency, and differentiation," *Biofabrication* **10**, 035005 (2018).
- ²¹D. Riester, J. Budde, C. Gach, A. Gillner, and M. Wehner, "High speed photography of laser induced forward transfer (LIFT) of single and double-layered transfer layers for single cell transfer," *J. Laser Micro Nanoeng.* **11**, 199–203 (2016).
- ²²T. Smausz, B. Hopp, G. Kecskeméti, and Z. Bor, "Study on metal microparticle content of the material transferred with absorbing film assisted laser induced forward transfer when using silver absorbing layer," *Appl. Surf. Sci.* **252**, 4738–4742 (2006).
- ²³A. Sorkio *et al.*, "Human stem cell based corneal tissue mimicking structures using laser-assisted 3D bioprinting and functional bioinks," *Biomaterials* **171**, 57–71 (2018).
- ²⁴S. Catros *et al.*, "Laser-assisted bioprinting for creating on-demand patterns of human osteoprogenitor cells and nano-hydroxyapatite," *Biofabrication* **3**, 025001 (2011).
- ²⁵L. Koch, O. Brandt, A. Deiwick, and B. Chichkov, "Laser-assisted bioprinting at different wavelengths and pulse durations with a metal dynamic release layer: A parametric study," *Int. J. Bioprinting* **3**, 42–53 (2017).
- ²⁶V. I. Yusupov *et al.*, "Laser-induced transfer of gel microdroplets for cell printing," *Quantum Electron.* **47**, 1158–1165 (2017).
- ²⁷A. Zennifer, A. Subramanian, and S. Sethuraman, "Design considerations of bioinks for laser bioprinting technique towards tissue regenerative applications," *Bioprinting* **27**, e00205 (2022).
- ²⁸N. R. Schiele, D. B. Chrisey, and D. T. Corr, "Gelatin-based laser direct-write technique for the precise spatial patterning of cells," *Tissue Eng., Part C* **17**, 289–298 (2011).
- ²⁹D. R. Bijukumar *et al.*, "Systemic and local toxicity of metal debris released from hip prostheses: A review of experimental approaches," *Nanomed. Nanotechnol. Biol. Med.* **14**, 951–963 (2018).
- ³⁰Q. Li, J. Lu, P. Gupta, and M. Qiu, "Engineering optical absorption in graphene and other 2D materials: Advances and applications," *Adv. Opt. Mater.* **7**, 1900595 (2019).
- ³¹J. Peña-Bahamonde, H. N. Nguyen, S. K. Fanourakis, and D. F. Rodrigues, "Recent advances in graphene-based biosensor technology with applications in life sciences," *J. Nanobiotechnol.* **16**, 1–17 (2018).
- ³²Y. Liu *et al.*, "Single-layer graphene enhances the osteogenic differentiation of human mesenchymal stem cells *in vitro* and *in vivo*," *J. Biomed. Nanotechnol.* **12**, 1270–1284 (2016).
- ³³M. Gu *et al.*, "Effects of thermal treatment on the adhesion strength and osteoinductive activity of single-layer graphene sheets on titanium substrates," *Sci. Rep.* **8**, 1–15 (2018).
- ³⁴J. Yan, Y. Huang, C. Xu, and D. B. Chrisey, "Effects of fluid properties and laser fluence on jet formation during laser direct writing of glycerol solution," *J. Appl. Phys.* **112**, 083105 (2012).
- ³⁵Z. Zhang, R. Xiong, D. T. Corr, and Y. Huang, "Study of impingement types and printing quality during laser printing of viscoelastic alginate solutions," *Langmuir* **32**, 3004–3014 (2016).
- ³⁶J. Mazumdar, *Biofluid Mechanics* (World Scientific, 2015).
- ³⁷J. M. Bourget *et al.*, "Patterning of endothelial cells and mesenchymal stem cells by laser-assisted bioprinting to study cell migration," *Biomed. Res. Int.* **2016**, 1–7 (2016).
- ³⁸R. Xiong, Z. Zhang, W. Chai, D. B. Chrisey, and Y. Huang, "Study of gelatin as an effective energy absorbing layer for laser bioprinting," *Biofabrication* **9**, 024103 (2017).
- ³⁹J. L. Curley *et al.*, "Isolated node engineering of neuronal systems using laser direct write," *Biofabrication* **8**, 015013 (2016).
- ⁴⁰S. Ahn *et al.*, "Evaluation of dynamic properties of sodium-alginate-reinforced soil using a resonant-column test," *Materials (Basel)* **14**, 2743 (2021).
- ⁴¹R. Sattler, C. Wagner, and J. Eggers, "Blistering pattern and formation of nanofibers in capillary thinning of polymer solutions," *Phys. Rev. Lett.* **100**, 164502 (2008).
- ⁴²P. P. Bhat *et al.*, "Formation of beads-on-a-string structures during break-up of viscoelastic filaments," *Nat. Phys.* **6**, 625–631 (2010).
- ⁴³M. S. N. Oliveira, R. Yeh, and G. H. McKinley, "Iterated stretching, extensional rheology and formation of beads-on-a-string structures in polymer solutions," *J. Non-Newtonian Fluid Mech.* **137**, 137–148 (2006).
- ⁴⁴J. König, S. Nolte, and A. Tünnermann, "Plasma evolution during metal ablation with ultrashort laser pulses," *Opt. Express* **13**, 10597 (2005).
- ⁴⁵S. Chu *et al.*, "Numerical investigation on multiple resonant modes of double-layer plasmonic grooves for sensing application," *Nanomaterials* **10**, 308 (2020).
- ⁴⁶S. Morozova, E. Hitimana, S. Dhakal, K. G. Wilcox, and D. Estrin, "Scattering methods for determining structure and dynamics of polymer gels," *J. Appl. Phys.* **129**, 071101 (2021).
- ⁴⁷S. Yoon *et al.*, "Inkjet-spray hybrid printing for 3D freeform fabrication of multilayered hydrogel structures," *Adv. Healthcare Mater.* **7**, 1800050 (2018).
- ⁴⁸S. Xu, S. Cai, and Z. Liu, "Thermal conductivity of polyacrylamide hydrogels at the nanoscale," *ACS Appl. Mater. Interfaces* **10**, 36352–36360 (2018).